Effects of interface broadening on far-infrared and Raman spectra of GaAs/AlAs superlattices

B. Samson,* T. Dumelow, A. A. Hamilton, T. J. Parker, S. R. P. Smith, and D. R. Tilley
Department of Physics, University of Essex, Colchester, Essex, CO4 3SQ United Kingdom

C. T. Foxon,† D. Hilton, and K. J. Moore‡
Philips Research Laboratories, Redhill, Surrey, RH1 5HA United Kingdom
(Received 17 January 1992)

A one-dimensional local-mode model is developed to describe phonons propagating normal to the layers of $(GaAs)_{n_1}/(AlAs)_{n_2}$ superlattices, in which the effects of broadening of the interfaces can be quantitatively described. The model is applied to the analysis of Raman scattering and far-infrared (FIR) measurements on short-period superlattices, $n_1=n_2=2,3,\ldots,8$, and is shown to give a good description of data in both the GaAs and AlAs optic-phonon regions using an interface width parameter W of 1.4 lattice units. The model also describes the intensities of Raman-scattering modes, FIR dielectric scattering strengths, and linewidths. The analysis demonstrates that the effects of interface broadening must be included in an accurate description of phonons in short-period superlattices, and gives a quantitative assessment of interface quality that is in agreement with x-ray measurements.

I. INTRODUCTION

The properties of phonons in semiconductor superlattices are well understood in principle, based experimentally on Raman measurements of the acoustic- and optic-phonon modes (see the review by Jusserand and Cardona[1]), and on the theoretical side by models ranging from simple one-dimensional (1D) to full 3D lattice dynamical calculations (see Mendendez,[2] Fasolino, Molinari and Kunc,[3] and references cited therein).

The fact that the interface between two semiconductors is far from ideal is well known, and the effect on the folded acoustic and confined optic phonons has been studied by a number of authors including Jusserand *et al.*,[4] Fasol *et al.*,[5] and Wicks, Bradshaw, and Radulescu.[6] More recently the apparent discrepancy between the measured frequencies of the confined longitudinal optic-phonon modes in short-period $(GaAs)_{n_1}$ $(AlAs)_{n_2}$ structures, where the layer thicknesses n_1 and n_2 are between 1 and 4 monolayers, and the predicted values have been largely explained by the effects of interface broadening (Baroni, Giannozzi, and Molinari[7]). However, it appears that the actual details of the interface roughness are rather complicated, taking a "bimodal" form with in-plane terrace lengths as large as 1000 Å claimed to occur alongside "atomic scale roughness" (Warwick *et al.*[8] and Gammon, Shaabrook, and Katzer[9]). Measurements by Jusserand *et al.* and Moison *et al.*[10] have shown the frequencies of the confined LO phonons to be a sensitive probe of the latter, which occurs largely at the "inverse" interface (GaAs on AlAs). Until recently little has been known about the effect of interface broadening on the TO modes (Scamarcio *et al.*[11]).

The theoretical modeling of these structures is complicated by the need to describe the phonon response of the interface alloy region that arises as a result of the broadening (Molinari *et al.*[12]). The phonon properties of $Al_xGa_{1-x}As$ alloys have received considerable attention recently, being described either by *ab initio* calculations (Baroni, de Gironcoli, and Gianozzi[13]) or approximation techniques such as the coherent potential approximation (CPA) (Jusserand, Pacquet, and Mollot,[14] and Kechrakos, Briddon, and Inkson[15]).

In this paper we outline the details of a simple 1D model for phonons propagating along the superlattice axis; the model is based on the next-nearest-neighbor linear chain model and is essentially an extension to the random element isodisplacement and pseudo unit cell models of Chang and Mitra.[16] As such, the model is capable of describing quantitatively the two-mode behavior of bulk $Al_xGa_{1-x}As$ alloys and the properties of confined phonon modes in short-period GaAs/AlAs superlattices. Comparison with the longitudinal- and transverse-optic (LO and TO) mode frequencies as measured by Raman and infrared reflectivity respectively gives excellent agreement, assuming that the interface broadening parameter (representing an effective broadening of the GaAs/AlAs interface in monolayer units) has the value $W=1.4$ for the samples used in our investigations. In addition, the model provides expressions for the Raman scattering strengths, the dielectric response (both ϵ_{xx} and ϵ_{zz}), and the confined mode linewidths, which we compare in detail with the far infrared reflectivity (FIR) data. The value obtained for the interface width parameter is in excellent agreement with x-ray analyses on similar samples. We conclude that our model provides a simple quantitative method of analyzing phonon modes and of characterizing short-period GaAs/AlAs superlattices.

II. LOCAL MODE MODEL

We describe here a local-mode for the description of phonons in GaAs/AlAs alloys and superlattices. A partial description of this model, with particular reference to

the derivation of LO frequencies, has already been published.[17] Our approach amounts to an extension of the "modified random-element isodisplacement" and "pseudo-unit-cell" models used by Chang and Mitra[16] in describing the long-wavelength response of random alloys. It is appropriate for alloys that show a two-mode behavior, in that the optic-phonon branches of GaAs and AlAs are entirely distinct in the alloy. The formalism reduces to a one-dimensional set of equations of motion, and the discussion here is restricted to phonons propagating along a [001] axis (i.e., along the superlattice growth direction), though the model could be extended to arbitrary directions of propagation. Interactions are restricted to nearest and next-nearest-neighbor forces, which are assumed in effect to incorporate the long-range electrostatic interactions. The principal theoretical models that have been used in the context of the lattice dynamics of alloys are the CPA, which has certain similarities with the local-mode model, but is essentially a perturbation theory model that cannot readily cope with the complete range of alloying, and the virtual-crystal approximation, which does not permit the description of an alloy response that shows the two-mode behavior.

The defining lattice-dynamical equations of motion take the form

$$-M_s\omega^2 u_{sn}=\sum_{s',n'}\{\mathcal{Y}_{ss'}^{nn'}(u_{s'n'}-u_{sn})\}+f_{sn} ,$$

where u_{sn} is the displacement coordinate for the atom of type s in the unit cell at position $\mathbf{R}_n$, $\mathcal{Y}$ is the force constant matrix, and f_{sn} a conjugate generating force acting on the site (s,n). In the GaAs (zinc-blend) lattice, the structure consists of planes of atoms of the same type s ($=A$ or B) normal to the cubic [001] axis, so in the special case of [001]-propagating phonons, all coordinates u_{sn} are the same for sites n in the same layer i and the problem can be reduced to a one-dimensional form in which u_{si} represents the displacement amplitude of s-type atoms in the ith layer. We use a linear-chain model which includes nearest- and next-nearest-neighbor interactions; the linear chain consists of a linear array of alternating A and B atoms, with nearest-neighbor A-B force constants C and next-nearest-neighbor force constants D (for A-A) and E (for B-B), as shown in Fig. 1. In order to describe the superlattice, the B atoms are allowed to be of two types, $s=1$ or 2 (corresponding to the Ga or Al sites, respectively), while the A atoms (As) are of a single type. The equation of motion for the ith B site is

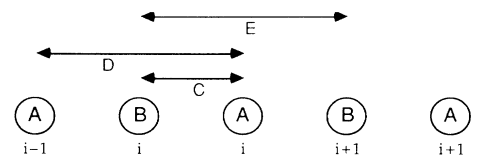

FIG. 1. Linear chain of A and B atoms, showing the nearest- and next-nearest-neighbor force constants.

$$-M_{Bi}\omega^2 u_{Bi}=\sum_j\{C^{ij}(u_{Aj}-u_{Bi})+E^{ij}(u_{Bj}-u_{Bi})\}+f_{Bi} , \quad (1)$$

where u_{si} are the appropriate displacement coordinates, f_{si} conjugate generating forces, M_{si} the masses, and the summation over j is restricted to nearest and next-nearest neighbors.

In the actual lattice, each linear-chain atom represents a *layer* of atoms, and the problem becomes much more complicated if there are atoms of different types within the same layer. In the virtual-crystal approximation, the force constants and masses are averaged, but this procedure is inappropriate because it simply leads to a single optic-mode response that cannot describe the two-mode behavior of an $Al_xGa_{1-x}As$ alloy. Instead, we use a procedure that in effect produces an average of the atomic responses, rather than an average of the force constants. The procedure starts from the local-mode response of an atoms in its local environment; the essence of this local-mode approximation lies in modifying Eq. (1) in order to represent the response of a layer of atoms rather than an individual atom. To do this, Eq. (1) is rewritten as

$$u_{Bi}=\chi_{Bi}\left[\sum_j\{C^{ij}u_{Aj}+E^{ij}u_{Bj}\}+f_{Bi}\right] , \quad (2)$$

with

$$\chi_{Bi}(\omega)=\frac{M_{Bi}^{-1}}{\omega_{Bi}^2-\omega^2}, \quad \omega_{Bi}^2=M_{Bi}^{-1}\sum_j\{C^{ij}+E^{ij}\} .$$

χ_{Bi} is the site susceptibility and ω_{Bi} its local-mode frequency. Equation (2) is then averaged in a physically suitable way over a layer i in which the probability of occupation of a B site by atom type s ($=1$ or 2) is P_{si} (with $P_{1i}+P_{2i}=1$). In the local-mode approximation, this average is performed as follows. The coordinate u_{Bi} is written as the weighted sum of two separate coordinates u_{1i} and u_{2i}

$$u_{Bi}=P_{1i}u_{1i}+P_{2i}u_{2i} . \quad (3)$$

u_{si} represents the average response of the s-type B atoms in layer i, and has an equation of motion of the form of Eq. (2)

$$u_{si}=\chi_{si}\left[\sum_j\left\{C_{sA}^{ji}u_{Aj}+\sum_{s'}E_{ss'}^{ij}u_{s'j}\right\}+f_{si}\right]$$

$$\text{with } \chi_{si}=\frac{M_s^{-1}}{\omega_{si}^2-\omega^2} , \quad (4)$$

where the extended notation $E_{ss'}^{ij}$ indicates the coupling between B sites of type s in layer i and B sites of type s' in layer j, and C_{sA}^{ji} similarly indicates the coupling between the A sites in layer j and the B sites of type s in layer i. In terms of the 1D force constants, these are given by

$$C_{sA}^{ji}=C_s, \text{ for nearest neighbors } i,j$$
$$E_{ss'}^{ij}=E_{ss'}P_{s'j} \text{ for next-nearest neighbors } i,j , \quad (5)$$

where the strength of the latter is taken as proportional to the probability of occupation of the adjacent layer j of a B-site atom of type s'. The term ω_{si}^2 in the susceptibility χ_{si} is determined simply by the condition that the uniform mode $u_{si}=$ const is a solution at $\omega=0$, i.e.,

$$\omega_{si}^2=M_s^{-1}\sum_j\left\{C_s^{ji}+\sum_{s'}E_{ss'}^{ij}\right\} . \tag{6}$$

Interactions between different atom types 1 and 2 in the same layer are introduced in the same way that Chang and Mitra[16] have done by including a force constant of the form

$$E_{ss'}^{ij}=HP_{s'i} \quad \text{for } i=j,\ s'=\bar{s} , \tag{7}$$

where we assume that the parameter H is independent of i. We will show later that a value for H can be derived by appeal to experiment. In effect, the local mode approximation involves replacing the susceptibility of the ith B layer by the average susceptibility $\chi_{Bi}\equiv\langle\chi_B\rangle_i=P_{1i}\chi_{1i}+P_{2i}\chi_{2i}$, a procedure which is justified because of the well-separated optic-phonon bands of GaAs and AlAs.

Similar considerations apply to the equation of motion for the A coordinate

$$u_{Ai}=\chi_{Ai}\left[\sum_j\left\{\sum_s C_{As}^{ij}u_{sj}+D^{ij}u_{Aj}\right\}+f_{Ai}\right] , \tag{8}$$

in which the nearest and next-nearest interactions are described by

$$C_{As}^{ij}=C_sP_{sj}, \quad D^{ij}=\sum_s D_sP_{sj'} , \tag{9}$$

where j' is the B layer between i and j. There is no analog of the self-energy interaction constant H for the A sites.

The equations of motion, written out explicitly for nearest and next-nearest interactions, are thus

$$\begin{aligned}
(\omega_{Ai}^2-\omega^2)u_{Ai}=&M_A^{-1}[\{C_1(P_{1i}u_{1i}+P_{1,i+1}u_{1,i+1})+C_2(P_{2i}u_{2i}+P_{2,i+1}u_{2,i+1})\\
&+D_1(P_{1,i+1}u_{A,i+1}+P_{1i}u_{A,i-1})+D_2(P_{2,i+1}u_{A,i+1}+P_{2i}u_{A,i-1})\}+f_{Ai}] ,\\
(\omega_{si}^2-\omega^2)u_{si}=&M_s^{-1}[\{C_s(u_{Ai}+u_{A,i-1})+E_{s1}(P_{1,i+1}u_{1,i+1}+P_{1,i-1}u_{1,i-1})\\
&+E_{s2}(P_{2,i+1}u_{2,i+1}+P_{2,i-1}u_{2,i-1})+HP_{\bar{s}i}u_{\bar{s}i}\}+P_{si}f_{Bi}] ,
\end{aligned} \tag{10}$$

with

$$\begin{aligned}
\omega_{Ai}^2=&M_A^{-1}[(C_1+D_1)(P_{1i}+P_{1,i+1})+(C_2+D_2)(P_{2i}+P_{2,i+1})] ,\\
\omega_{si}^2=&M_s^{-1}[2C_s+E_{s1}(P_{1,i+1}+P_{1,i-1})+E_{s2}(P_{2,i+1}+P_{2,i-1})+HP_{\bar{s}i}] .
\end{aligned}$$

The set of equations (10) represents the response of a 1D infinite chain; the set can be restricted by looking for solutions, corresponding to a wave vector Q, that satisfy the Bloch condition for cyclical boundary conditions, i.e., $u_{s,i+N}=\exp(2\pi iQ)u_{si}$. Q is the reduced wave vector in units $2\pi/Na$, so that the real wave vector is $q=(2\pi/Na)Q$, where a is the bulk monolayer lattice parameter and N the number of monolayers in the superlattice unit cell. Thus Eq. (10) describes the coupled equations of motion of the $3N$ variables u_{Ai}, u_{1i}, and u_{2i}, providing $3N$ normal-mode solutions at wave vector Q. Note that if the superlattice is pure GaAs/AlAs, with sharply defined layers and no alloying, there would only need to be $2N$ equations of motion in (10); the possibility of alloying introduces the extra N modes (which will of course have zero intensity of response in the limit of zero alloying).

Formally, it is convenient to symmetrize the equations of motion by defining normalized coordinates

$$\begin{aligned}
&e_{Ai}=u_{Ai}\sqrt{M_A}, \quad e_{si}=u_{si}\sqrt{M_sP_{si}},\\
&f'_{Ai}=f_{Ai}/\sqrt{M_A}, \quad f'_{si}=f_{si}\sqrt{P_{si}/M_s} .
\end{aligned} \tag{11}$$

The equations of motion are given by

$$(\mathbf{Y}-\omega^2\mathbf{I})\cdot\mathbf{e}=\mathbf{f}' , \tag{12}$$

where $\mathbf{Y}$ is the $3N\times3N$ Hermitian coupling matrix and $\mathbf{I}$ the identity matrix; the elements of the matrix $\mathbf{Y}$ are listed in the Appendix. It is convenient to use a single index n to represent the combination of layer index i and species index (A, 1, or 2). Let $v_{n\mu}$ be the unitary matrix that diagonalizes $\mathbf{Y}$, with eigenvalues ω_μ^2, i.e.,

$$\sum_{n'}Y_{nn'}v_{\mu n'}=v_{n\mu}\omega_\mu^2 \quad \text{with} \sum_n v_{n\mu}^*v_{n\mu'}=\delta_{\mu\mu'} ,$$

then the formal solution of Eq. (12) is

$$e_n=\sum_{\mu,n'}\frac{v_{n\mu}v_{n'\mu}^*}{\omega_\mu^2-\omega^2}f'_{n'} , \tag{13}$$

applicable for each wave vector Q.

A. Light-scattering intensities and dielectric susceptibility

In most cases of interest, the force on each site n (where, for convenience, the single index n does duty for

the two site indices s and j) can be written in terms of a single force with amplitude F and wave vector Q as

$$f_n(Q)=\alpha_n F\exp(2\pi iQz_n)$$

or (14)

$$f'_n(Q)=\gamma_n F\exp(2\pi iQz_n)\ ,$$

where α_n and γ_n are appropriate coupling coefficients [related by the normalization of Eq. (11)] and $z_n\equiv z_{sj}$ is the coordinate of the site of type s in cell j. Q is taken in units $2\pi/Na$ (spanning the range $-\frac{1}{2}<Q\leq\frac{1}{2}$), and z_n is in lattice units a. The response conjugate to this force is

$$R(Q)=\sum_n \alpha_n^* u_n P_n\exp(-2\pi iQz_n/N)\ , \tag{15}$$

and the total susceptibility response function (per atomic unit cell) is

$$G(Q,\omega)=\frac{1}{N}\frac{\partial R}{\partial F}=\frac{1}{N}\sum_\mu \frac{1}{\omega_\mu^2-\omega^2}\left|\sum_n \gamma_n^* v_{n\mu}\exp(-2\pi iQz_n/N)\right|^2\ , \tag{16}$$

where we use Eqs. (11) and (13)–(15) to obtain the final expression.

The function (16) can be used to represent both the dielectric susceptibility and the Raman-scattering response. Consider the former first. Suppose that there are appropriate effective charges $\pm q_s^D$ for the A and B sites, respectively, for the two types of lattice s, and take the effective charge at the jth A site as the average of the contributions from the neighboring B sites:

$$q_{Aj}^D=\tfrac{1}{2}[q_1^D(P_{1j}+P_{1,j+1})+q_2^D(P_{2j}+P_{2,j+1})]\ . \tag{17}$$

Then the response is

$$R(Q)=\sum_{j=1}^{N}[q_{Aj}^D u_{Aj}-(q_1^D P_{1j}u_{1j}+q_2^D P_{2j}u_{2j})e^{\pi iQ/N}]\times e^{-2\pi iQj/N} \tag{18}$$

(with $z_{Aj}=j$ and $z_{Bj}=j-\frac{1}{2}$). This leads to expressions for the coupling coefficients

$$\gamma_{sj}=-q_s^D\sqrt{P_{sj}/M_s}\,e^{\pi iQ/N}$$
$$\gamma_{Aj}=[q_1^D(P_{1j}+P_{1,j+1})+q_2^D(P_{2j}+P_{2,j+1})]/2\ . \tag{19}$$

The quantity R in Eq. (18) is now proportional to the macroscopic polarization $\mathcal{P}_u$ of the atomic motion induced by the applied field F:

$$\mathcal{P}_u=\frac{R}{a^3}=\frac{G(Q,\omega)}{a^3}F\ , \tag{20}$$

where a^3 is the volume of the atomic unit cell. In an experiment involving an external electric field $\mathcal{E}_0$ applied normal to the superlattice, the appropriate internal field F is $\mathcal{D}/\epsilon_0$ (the field in a disk-shaped cavity oriented normal to a uniform field in a dielectric). In the spirit of the effective medium model used by Dumelow *et al.*,[18] the displacement vector $\mathcal{D}$ is uniform throughout the system; it can be written as $\mathcal{D}=\epsilon_{zz}^\infty\epsilon_0\mathcal{E}+\mathcal{P}_u=\epsilon_{zz}\epsilon_0\mathcal{E}$, where ϵ_{zz}^∞ includes polarization contributions from other sources. Thus the longitudinal dielectric function for response normal to the superlattice planes is

$$\frac{1}{\epsilon_{zz}(Q,\omega)}=\epsilon_0\frac{\partial\mathcal{E}}{\partial\mathcal{D}}=\frac{1}{\epsilon_{zz}^\infty}\left[1-\frac{\partial\mathcal{P}_u}{\partial\mathcal{D}}\right]=\frac{1}{\epsilon_{zz}^\infty}\left[1-\frac{G(Q,\omega)}{a^3\epsilon_0}\right]\ . \tag{21}$$

The effective charges q_s^D can be estimated from the bulk-lattice dielectric functions. For example, in a bulk lattice of type s, the lattice phonon model gives

$$G(0,\omega)=\frac{(q_s^D)^2}{2C_s}\frac{(\omega_{0s}^{\rm L})^2}{(\omega_{0s}^{\rm L})^2-\omega^2}=(q_s^D)^2\frac{M_A^{-1}+M_s^{-1}}{(\omega_{0s}^{\rm L})^2-\omega^2}\ , \tag{22}$$

where $\omega_{0s}^{\rm L}$ is the zone-center LO frequency of lattice s. This leads to the usual form for the dielectric function

$$\epsilon(\omega)=\frac{(\omega_0^{\rm L})^2-\omega^2}{(\omega_0^{\rm T})^2-\omega^2}\epsilon^\infty \tag{23}$$

so long as the effective charge q_s^D is given by

$$(q_s^D)^2=2C_s a^3\epsilon_0\frac{(\omega_{0s}^{\rm L})^2-(\omega_{0s}^{\rm T})^2}{(\omega_{0s}^{\rm L})^2}=a^3\epsilon_0\frac{(\omega_{0s}^{\rm L})^2-(\omega_{0s}^{\rm T})^2}{M_A^{-1}+M_s^{-1}}\ , \tag{24}$$

with $\omega_{0s}^{\rm T}$ the TO zone-center frequency for lattice s.

One can associate a response strength S_μ with the superlattice mode of frequency ω_μ by rewriting Eq. (21) as a sum over the individual mode responses:

$$\frac{1}{\epsilon_{zz}(Q,\omega)}=\frac{1}{\epsilon_{zz}^\infty(Q)}\left[1-\sum_\mu\frac{S_\mu^{\rm L}(Q)}{\omega_\mu^{\rm L}(Q)^2-\omega^2}\right]\ , \tag{25}$$

with

$$S_\mu^{\rm L}(Q)=\frac{1}{Na^3\epsilon_0}\left|\sum_n \gamma_n^* v_{n\mu}e^{-2\pi iQz_n/N}\right|^2\ .$$

The coefficients γ_n are given by Eq. (19), with q_s^D given by (24). It is normally appropriate to put $Q=0$.

If, instead of considering the longitudinal response, one considers the transverse dielectric response, the analysis is very similar, with appropriate redefinition of the quantities involved. With an external field $\mathcal{E}_0$ applied parallel to the superlattice planes, the applied field is just $F=\epsilon_{xx}^\infty\mathcal{E}_0$, the internal field $\mathcal{E}=\mathcal{E}_0$ is uniform throughout the system, and the displacement vector is $\mathcal{D}=\epsilon_{xx}^\infty\epsilon_0\mathcal{E}+\mathcal{P}_u=\epsilon_{xx}\epsilon_0\mathcal{E}_0$; thus the transverse dielectric

response is

$$\epsilon_{xx}(Q,\omega)=\frac{1}{\epsilon_0}\frac{\partial\mathcal{D}}{\partial\mathcal{E}}=\epsilon_{xx}^{\infty}(Q)\left[1+\frac{G(Q,\omega)}{a^3\epsilon_0}\right]$$
$$=\epsilon_{xx}^{\infty}(Q)\left[1+\sum_{\mu}\frac{S_{\mu}^{\mathrm{T}}(Q)}{\omega_{\mu}^{\mathrm{T}}(Q)^2-\omega^2}\right], \quad (26)$$

analogous to Eq. (25). This expression, with poles at the transverse frequencies, again leads to the expression (23) for the bulk dielectric response if the coupling charges q_s^D are given by the expression (24) using the appropriate effective transverse parameters.

A similar analysis can be used for the Raman-scattering strengths. Here we are interested in the scattering function

$$I(Q,\omega)=\pi^{-1}\,\mathrm{Im}\{G(Q,\omega)\}$$
$$=\sum_{\mu}I_{\mu}(Q)[\delta(\omega-\omega_{\mu})-\delta(\omega+\omega_{\mu})], \quad (27)$$

where the δ functions become Lorentzian line-shape functions when damping is included. The scattering strength of the mode at frequency ω_{μ} is

$$I_{\mu}(Q)=\frac{1}{N\omega_{\mu}(Q)}\left|\sum_{n}\gamma_n^{*}v_{n\mu}e^{-2\pi iQz_n/N}\right|^2. \quad (28)$$

There are several possible mechanisms for the Raman-scattering intensity, leading to different forms for the coefficients γ_{sj}. In the optic-phonon region under non-resonant excitation, the dominant interaction mechanism involves the deformation potential, which can be approximately modeled by using coupling coefficients of a form similar to that of Eq. (19), though with different effective charges q_s^R. The latter can be parametrized by noting that the model gives the strength of the LO mode in bulk lattice s as

$$I_s=\frac{(q_s^R)^2\omega_{0s}}{2C_s}. \quad (29)$$

In Raman scattering, only the relative rather than absolute scattering strengths are measurable, so one needs only the relative scattering strengths I_2/I_1 of the pure materials in order to obtain the ratio of the effective charges q_2^R/q_1^R.

This procedure gives a first approximation appropriate for the treatment of Raman-scattering intensities in the optic-mode region. However, in the acoustic-phonon region, the principal scattering mechanism involves the photoeleastic coupling, while in resonant Raman scattering, the Fröhlich interaction produces a coupling proportional to the displacement gradient at each atomic site, with a behavior somewhat similar to the photoelastic interaction. The details of the coupling are outside the scope of the present paper.

We have adopted a somewhat similar procedure to that used for estimating the mode intensities in order to estimate the mode linewidths. The procedure is described below, and uses a semiempirical approach that includes the effects of alloying at the interfaces.

To a first approximation, one can assume that each atom, of type S ($=A$, 1, or 2) and layer index i, gives a contribution to the damping parameter Γ_{μ} of the mode μ of the form $\Delta\Gamma_{Si,\mu}=\Gamma_S|v_{Si,\mu}|^2$, proportional to the vibrational contribution $|v_{Si,\mu}|^2$ from each atom of type S, where Γ_S is a constant. However, this expression neglects the inhomogeneous damping caused by the alloying. In a $Al_xGa_{1-x}As$ alloy, the simplest statistical approach to the effect of the alloying on the linewidth shows that the linewidth Γ_x is proportional to the concentration variance $(\Delta x)^2=x(1-x)$, i.e., $\Gamma_x\approx\Gamma_x^0x(1-x)$, where Γ_x^0 is a constant. This suggests the following simple approximation to the overall linewidth Γ_{μ} of the ($Q=0$) superlattice mode of index μ, which we have used in the analysis of our experimental data:

$$\Gamma_{\mu}=\sum_i\{\Gamma_{\mathrm{As}}|v_{Ai,\mu}|^2+\Gamma_{\mathrm{Ga}}|v_{1i,\mu}|^2+\Gamma_{\mathrm{Al}}|v_{2i,\mu}|^2$$
$$+\Gamma_x^0P_{1i}P_{2i}[|v_{1i,\mu}|^2+|v_{2i,\mu}|^2]\}, \quad (30)$$

where Γ_{As}, Γ_{Ga}, and Γ_{Al} are the natural damping parameters for the As, Ga, and Al atoms, respectively, and the last term depends on the product of the occupation probabilities $P_{1i}P_{2i}=x_i(1-x_i)$ for the layer i.

B. Modes and mode symmetries

The superlattice has $N=n_1+n_2$ monolayers in its unit cell; in this analysis there are three coordinates per monolayer, leading to a total of $3N$ distinct phonon modes, N acoustic and $2N$ optic. Of the $2N$ optic modes, only N are present as conventional GaAs or AlAs confined modes—n_1 in the GaAs layer and n_2 in the AlAs layer; the remaining N modes have zero intensity if the interfaces are perfectly defined, but appear as alloylike modes in the interfacial regions when broadening is present.

The basic symmetry of a simple GaAs/AlAs superlattice is D_{2d}. The $Q=0$ superlattice modes can be classified as either even or odd displacements with respect to reflection in a mirror plane midway between the interfaces (more precisely described as B_2 or A_1, respectively, under the D_{2d} superlattice symmetry). The N conventional confined optic-phonon modes are classified in terms of the mode index m—the number of displacement maxima (antinodes) in the confining layer. Conventional confined modes with odd or even index m have $Q=0$ symmetries B_2 or A_1, respectively. Only the B_2 modes can contribute to either the dielectric susceptibility or the deformation-potential induced light scattering intensity, so the only contributions from these modes will come from modes for which the index m is odd. These basic conclusions may, however, be modified in cases where the superlattice construction is more complicated or where the interface broadening is not symmetrical in the growth direction, because the overall lattice symmetry is then lower than D_{2d} with the result that contributions from even m modes to the dielectric susceptibility and the Raman scattering may be possible. It is also possible to observe Raman scattering from optic modes with even index m under near-resonant excitation conditions; our

model is not applicable here, but our experiments were all carried out under nonresonant conditions.

C. Bulk-lattice parametrization

Using the model outlined above, the eigenmodes of the bulk lattice of type s are solutions of the equation

$$[2M_s^{-1}\{C_s+E_{ss}[1-\cos(2\pi Q)]\}-\omega^2]\times[2\{C_s+D_s[1-\cos(2\pi Q)]\}-\omega^2]-4\cos^2(\pi Q)C_s^2/M_s=0 \quad (31)$$

with Q in the range $-\frac{1}{2}$ to $\frac{1}{2}$, and where we use units such that $M_A=1$. This gives the following special solutions:

(i) Zone center $Q=0$: $\omega_{0s}^2=2C_s(1+M_s^{-1})$.

(ii) Zone boundary ($Q=\frac{1}{2}$) optic mode: $\omega_{Zs}^2=(2/M_s)(C_s+2E_{ss})$.

(iii) Zone boundary ($Q=\frac{1}{2}$) acoustic mode: $\omega_{As}^2=2(C_s+2D_s)$.

(iv) Local mode of isolated B_s atoms in the $\bar{s}$ lattice: $\omega_{ls}^2=M_s^{-1}(2C_s+2E_{s\bar{s}}+H)$.

The expression (iv) is obtained from Eq. (7) with $P_s=0$.

In modeling the phonon dispersion curves for GaAs/AlAs superlattices, we have chosen to use experimental data on [001]-propagating bulk longitudinal and transverse phonons in order to specify the parameters necessary for the model. Eight phonon-mode frequencies are used, four frequencies (i)–(iv) as above for GaAs ($s=1$) and four for AlAs ($s=2$). There are ten parameters in the model (M_s, C_s, E_{ss}, and D_s for each lattice, plus the Ga-Al coupling E_{12} and self-interaction constant H), though only the sum $E'_{12}=(E_{12}+H/2)$ is available from experiment, leaving nine independent parameters. The precise choice of parameters is not crucial so long as a satisfactory representation of the phonon dispersion is obtained. We adopt the procedure of fixing M_1 (the $m_{\mathrm{Ga}}/m_{\mathrm{As}}$ mass ratio) at the atomic value $M_1=0.931$, and determining the remaining eight constants (C_1, E_{11}, D_1, M_2, C_2, E_{22}, D_2, and E'_{12}). E_{12} is determined from the simple average $E_{12}=(E_{11}+E_{22})/2$, from which H is obtained as $H=2(E'_{12}-E_{12})$.

The model parameters are specified in Table I, using frequencies appropriate to 77 K. Wherever temperature corrections were required, we assume

$$\frac{1}{\omega}\frac{d\omega}{dT}=-4.8\times10^{-5}\ \mathrm{K}^{-1} \quad \text{for GaAs-like modes,}$$

and

$$\frac{1}{\omega}\frac{d\omega}{dT}=-3.6\times10^{-5}\ \mathrm{K}^{-1} \quad \text{for AlAs-like modes,}$$

in line with the work of Jusserand and Sapriel.[19] Our own FIR or Raman measurements were used for all zone-center bulk parameters, although for AlAs-like modes we had to approximate bulk values to those of 75-Å barriers in a multiple-quantum-well structure. The FIR data of Kim and Spitzer[20] were used to obtain local-mode frequencies, and the accurate recent neutron-scattering measurements of Strauch and Dorner[21] to obtain all GaAs zone-boundary frequencies. Zone-boundary frequencies for AlAs are only available from optical measurements;[22,23] we use the optical absorption data of Onton and Chicotka[22] since they appear to be the more accurate. We must emphasize that, as is usual in lattice-dynamical analyses of this type, the model parameters are effective parameters which are not to be taken literally in an *ab initio* sense—they are simply parameters which realistically model those bulk properties that are important in the analysis of the superlattice phonons, namely the bulk [001] dispersion and the bulk alloy phonons. However, it should be remarked that the absence of a treatment of long-range Coulomb forces is not a serious defect in the present formulation concerning only [001]-propagating phonons, since it has been shown[24] that in this particular case the long-range Coulomb forces make no contribution and the phonons can be adequately represented by nearest and next-nearest neighbor effective interactions.

TABLE I. Bulk GaAs and AlAs mode frequencies at 77 K as used for deriving the model parameters used in the data analysis.

		Frequencies (cm^{-1})				Model parameters				
Lattice	Mode	ω_0	ω_Z	ω_l	ω_A	M_s	C_s	D_s	E_{ss}	H
GaAs	LO	295.0[a]	239.2[b]	254.7[c]	223.6[b]	0.9310	20979	2010	2828	7142
AlAs	LO	404.1[d]	395.0[e]	361.9[c]	213.2[e]	0.6161	31126	−4200	8468	
GaAs	TO	271.3[a]	255.5[b]	254.7[c]	81.4[b]	0.9310	17743	−7215	6322	15130
AlAs	TO	365.5[f]	331.1[e]	361.9[c]	104.5[e]	0.6141	23804	−9172	3457	

[a] FIR on GaAs substrates (this work).
[b] Neutron scattering (Strauch and Dorner Ref. 21).
[c] FIR on $Al_xGa_{1-x}As$ alloys (Kim and Spitzer, Ref. 20).
[d] Raman on GaAs/AlAs MQW barriers (this work).
[e] Optical absorption (Onton and Chicotka, Ref. 22).
[f] FIR on GaAs/AlAs MQW barriers (this work).

It is worth noting that this local-mode model can easily be used to find the frequencies of the alloy modes of a $Al_xGa_{1-x}As$ alloy, in effect as an $N=1$ superlattice. At the zone center, $Q=0$, the frequencies of the alloy modes are solutions of the equation

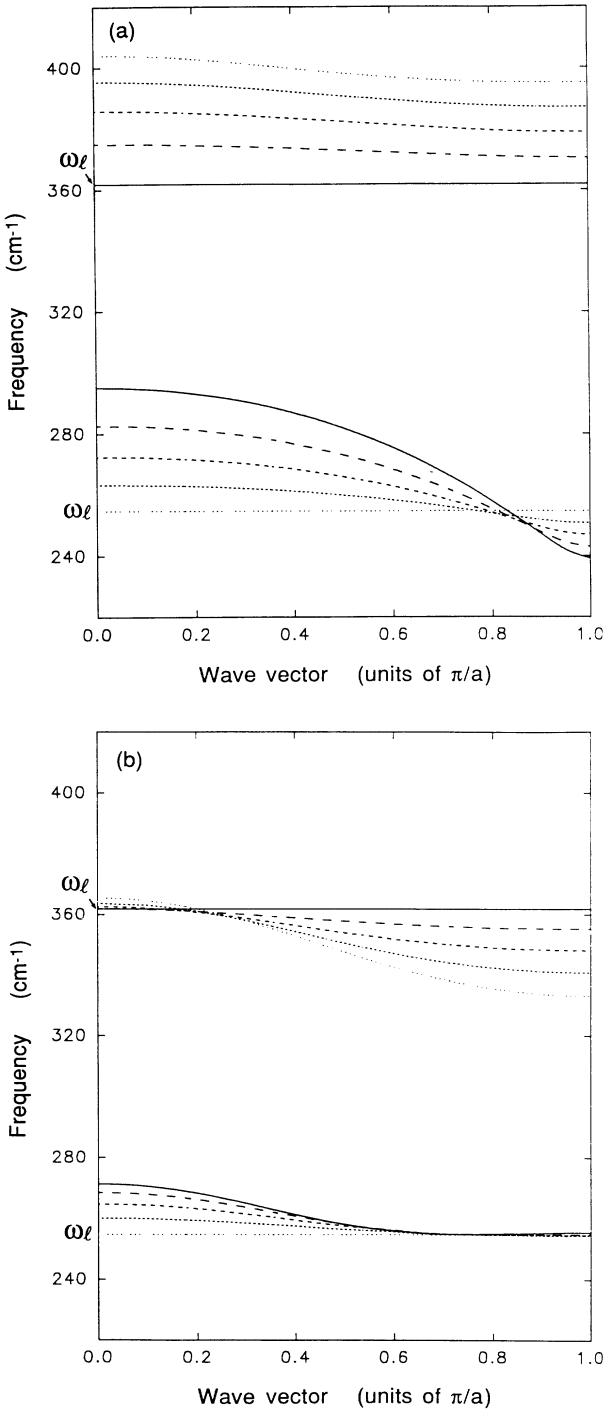

FIG. 2. Calculated dispersion curves for [001] phonons for the alloy $Al_xGa_{1-x}As$ using the model parameters in Table I for $T=77$ K: (a) LO modes; (b) TO modes. The values of concentration x are $x=0$(——); $x=0.25$(— — —); $x=0.5$(---); $x=0.75$(. . .); $x=1$(· · · · · · · · ·).

$$[\omega^2-x\omega_{l1}^2-(1-x)\omega_{01}^2][\omega^2-(1-x)\omega_{l2}^2-x\omega_{02}^2]$$
$$=4x(1-x)[C_1-E'_{12}/M_2][C_2-E'_{12}/M_1]\ . \quad (32)$$

Figure 2 shows the LO and TO dispersion curves of the alloy $Al_xGA_{1-x}As$ as a function of Ga concentration x for wave vector Q along [001]. Note the difference in behavior of the Ga-like and Al-like optic LO branches: since the local mode of Ga in AlAs lies within the GaAs optic band, the GaAs-like alloy dispersion curves all cross the $x=1$ curve (at the Ga local-mode frequency ω_l), losing their dispersion as $x\to 1$. On the other hand, the Al in GaAs local-mode frequency is below the AlAs optic-phonon band, so the dispersion curves of the different alloys do not cross in the AlAs-like region. These features of the alloy dispersion curves have also been demonstrated in full lattice-dynamical calculations.[13] The details of Fig. 2 correspond well with the experimental measurements of Jusserand, Pacquet, and Mollot,[14] and also with their CPA theoretical model for the alloy dispersion. However, we should point out that the fact that our model is only one-dimensional means that we obtain no contributions to the alloy modes from phonon branches other than [001], a detail which may have some significance for AlAs where the optic-phonon dispersion curves are highly anisotropic;[7] this will affect both the frequency and linewidth of the optic-phonon modes in the alloy.

In the case of the TO modes, the bulk dispersion curve comes closer to the local-mode frequency than for the LO modes, and the effect of alloying is less dramatic.

D. Interfacial broadening

In order to illustrate the effect of interfacial broadening, a model is used in which the broadening is represented by an error function, such that the probability that a B site a distance z from an AlAs/GaAs interface is occupied by a Ga atom is

$$P_1(z)=[1+\mathrm{erf}\{z/W\}]/2\ , \quad (33)$$

where W, the broadening parameter, represents the width of the interface in the lattice parameter units a, $z>0$ corresponds to the GaAs region and $z<0$ corresponds to the AlAs region. The error function does of course represent the type of broadening of an interface that would be caused by one-dimensional diffusion, but we are assuming that this form is also appropriate to describe the statistical nature of the effective broadening of an interface caused by interface roughness. Evidence that the actual interfaces are more complicated than this simple model is found in the work of Moison *et al.*[10] and Jusserand *et al.*[10]

This approach can be generalized for the purpose of describing a superlattice with arbitrary Ga and Al concentrations, e.g., $Al_xGa_{1-x}As/Al_yGa_{1-y}As$ superlattices. We have also investigated the effects of taking different interface parameters W at each interface, because it is expected that as-grown samples have a larger interface width for the "inverse" interface GaAs on AlAs than for the "normal" AlAs on GaAs interface: as a

rough generalization, this has little effect on mode frequencies (which occur as for the average interface width $\overline{W}$), but primarily affects the mode intensities (for example, even index m modes that are absent for the symmetric superlattice can be nonzero intensities for asymmetrically broadened interfaces). However, the following discussion assumes nominally pure Ga As/AlAs superlattices, for which the concentrations of Ga in the layers are $x=1$ or 0, and uniformly broadened interfaces.

E. Comparison of model with interface diffusion data

As an illustration of the model, Fig. 3 shows how an increase in the value of the interface parameter W affects the first nine GaAs confined modes of a $n_1=17$, $n_2=8$ superlattice. The essential feature to note is the way in which the frequencies move from a curve towards a straight line as W increases. This characteristic was noted by Levi *et al.*[25] when showing that an annealing treatment (around 3 h at 850 °C) produces interfacial diffusion, and the data in Fig. 2 are chosen to account for their experimental data. These authors followed Jusserand *et al.*[4] in using a well-shape parameter.

$$\rho=\frac{\omega_5-\omega_3}{\omega_3-\omega_1} \tag{34}$$

in order to characterize the curvature, where ω_m is the frequency of the mth-order confined mode. For a simple quadratic dispersion curve, one expects $\rho=2$, while $\rho=1$ for a straight line. On our model, the values $W=0$, 1.3, 3.4, and 5 correspond to values of $\rho=2.2$, 2.0, 1.35, and 1, respectively, and we therefore conclude that the "as grown" sample of Levi *et al.* had a value of $W=1.3$ ($\rho=2$), which increased to $W=3.4$ ($\rho=1.35$) after heat treatment. Note that $W=0$ does not in fact give $\rho=2$, in agreement with the actual GaAs dispersion curve measured by neutron scattering,[21] which is rather flat near the zone center and is better approximated by a value $\rho=2.2$.

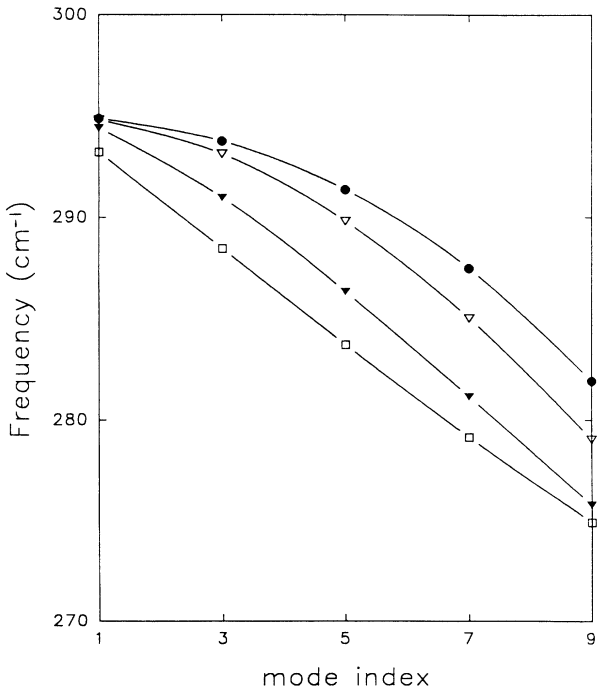

FIG. 3. Illustration of the effect of interfacial broadening on the GaAs-like confined modes of index $m=1-9$ for a $(GaAs)_{17}/(AlAs)_8$ superlattice. The values of broadening parameter W are 0.0(●), 1.3(▽), 3.3(▼), 5.0(□).

Our model therefore provides a quantitative assessment of the interfacial broadening. As a check on the actual numbers obtained, we derive a value for the diffusion coefficient (for interdiffusion of Ga and Al) of 8×10^{-20} $cm^2\,sec^{-1}$ at 850 °C, similar to the values around 2×10^{-20} $cm^2\,sec^{-1}$ obtained from optical absorption and x-ray diffraction data by Fleming *et al.*[26]

III. RAMAN AND INFRARED EXPERIMENTAL MEASUREMENTS AND COMPARISONS WITH LOCAL MODE MODEL

All samples were grown by molecular-beam epitaxy (MBE) in the same equipment. In each case 1 μm of superlattice, bounded by 0.1-μm GaAs cladding layers, was grown on a GaAs substrate maintained at 630 °C. The top cladding layer was removed for Raman measurements. Photoluminescence and photoluminescence-excitation data on samples from the same batch have been previously published,[27] and previous x-ray diffraction analysis has shown samples grown as part of the same batch to have nominally the same interface width.

Raman-scattering measurements were made using a standard double monochromator with photon-counting detection. The illumination source was an argon-ion laser (operating at 488 or 514.5 nm), and the nominal sample temperatures were room temperature or 77 K. Excitation was observed in backscattering geometry, with polarization analysis for $z(xy)\bar{z}$ (B_2) or $z(xx)\bar{z}$ (A_1) scattering.

FIR measurements were performed using a modified National Physical Laboratory/Grubb Parsons cube interferometer,[28] operated under laser control. The interferometer output was focused onto the sample, maintained at a nominal temperature of 77 K, at an incident angle of 45°, and the reflected signal refocused and detected using a Golay cell. A polarizer was placed in front of the detector so that either s- or p- polarized reflected light could be measured.[29]

A. Raman measurements of confined optic phonons in short-period superlattices

Figure 4 shows a comparison of the model with experimental measurements using Raman scattering of confined optic phonons in short-period $(GaAs)n_1/(AlAs)n_2$ superlattices, with values for $n_1=n_2=8$, 6, 5, 4, 3, and 2 and the 50% alloy. The value $W=1.4$ gives a best fit to the data. The solid curves in Fig. 4 show the bulk phonon curves produced by the model parameters defined in Table I [as produced by Eq. (31)], plotted vs wave vector Q in units of π/a. In the basic nearest-neighbor 1D model, Jusserand and Pacquet[30] pointed out that the frequen-

cy of the confined mode of index m in layer s (containing n_s lattice periods) corresponds approximately to that of a bulk mode of wave vector $m\pi/a(n_s+1)$. In order to provide an indication of the correspondence between the superlattice and the bulk frequencies, we have therefore plotted the confined superlattice modes in Fig. 4(a) at the bulk wave vectors

$$q_{ms}=\frac{m}{n_s+0.8}\frac{\pi}{a}\ , \tag{35}$$

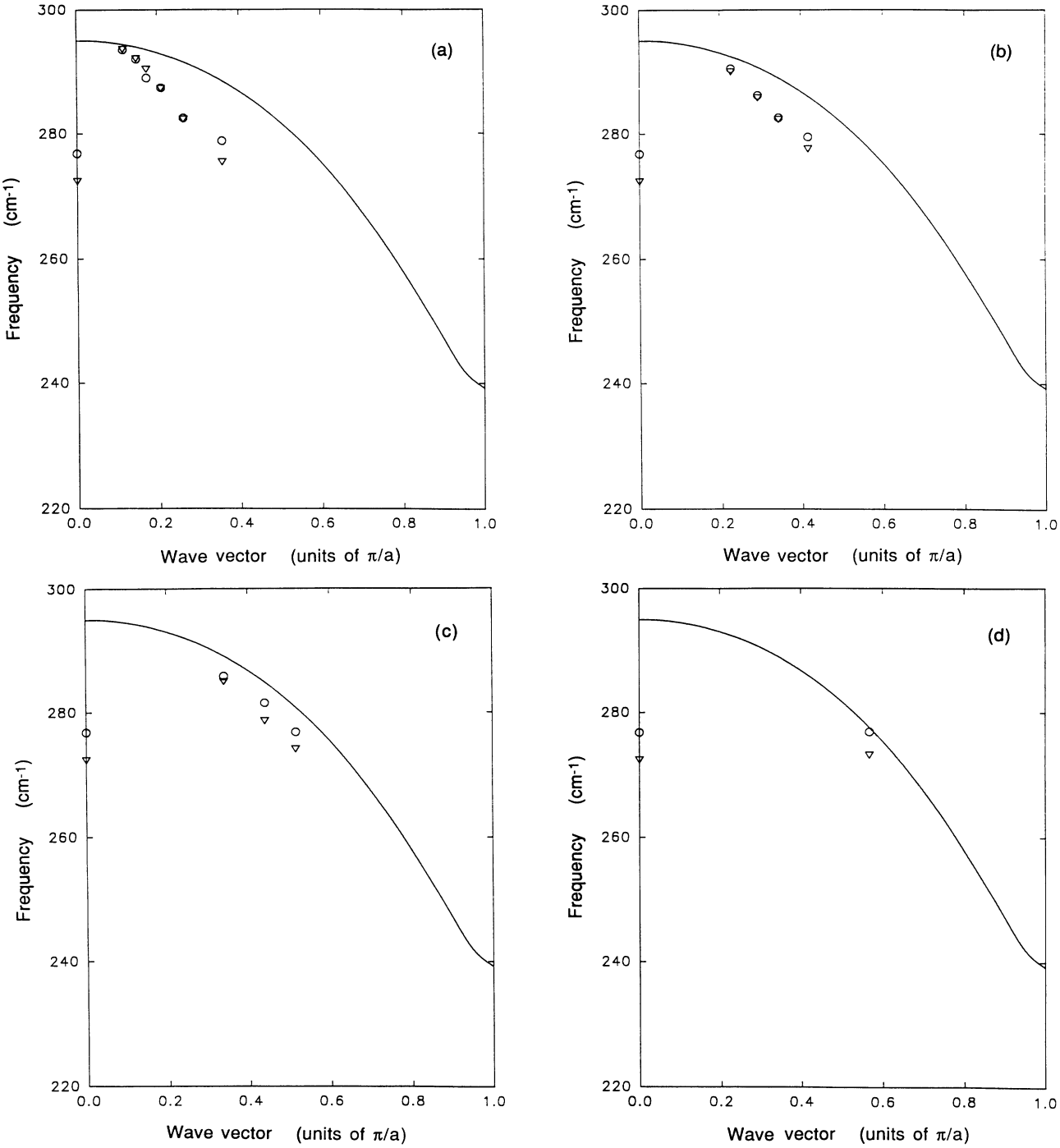

FIG. 4. LO confined mode frequencies in short-period $(GaAs)_n/(AlAs)_n$ superlattices as measured by Raman scattering (○) and as calculated for $W=1.4$(▽). The data pairs for modes of index m are shown at effective wave vector $q=m/(n+0.8)$. The solid curves show the bulk dispersion curves for the parameters given in Table I. (a) GaAs-like $m=1$; (b) GaAs-like $m=2$; (c) GaAs-like $m=3$; (d) GaAs-like $m=5$; (e) AlAs-like $m=1$. In each case the alloy $Al_{0.5}Ga_{0.5}As$ is shown for reference at $q=0$, followed by the superlattice data (from left to right) corresponding to $n=8$, 6, 5, 4, 3, and 2 (modes associated with the lower n values are not observed in all cases).

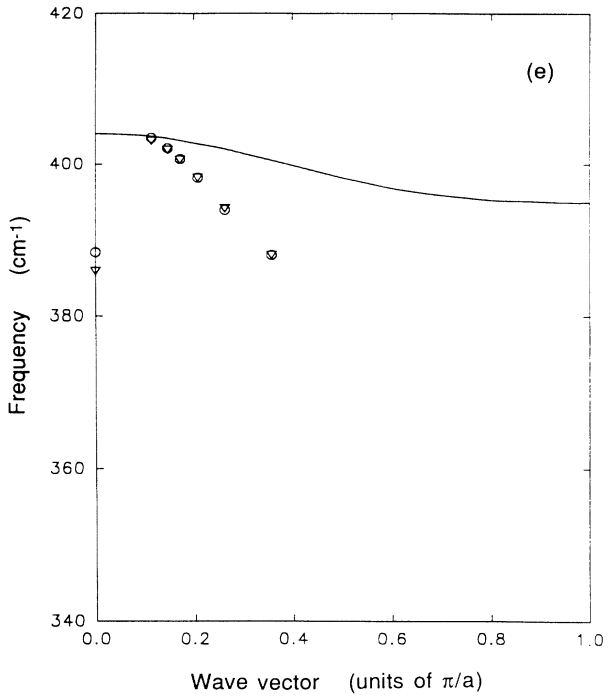

FIG. 4. (*Continued*).

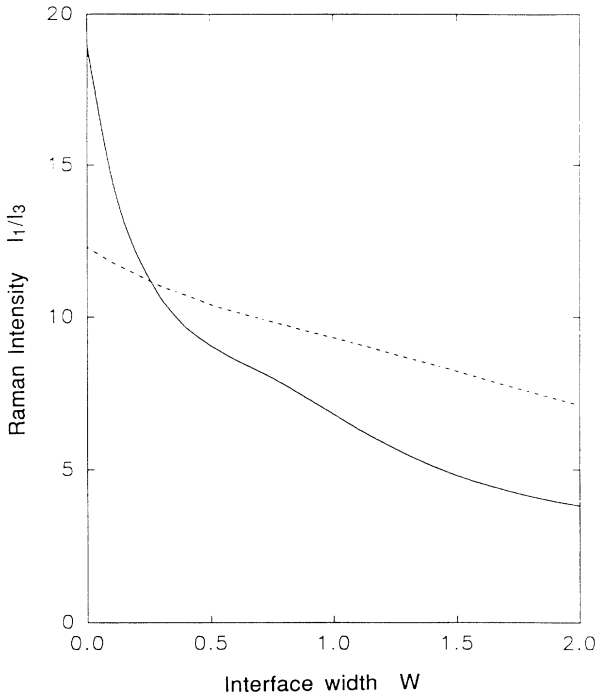

FIG. 5. Ratio of Raman-scattering intensities of the $m=1$ and 3 confined optic phonons as a function of interface width W for a $(GaAs)_7/(AlAs)_7$ superlattice: GaAs-like LO modes (——), GaAs-like TO modes (---).

where the value 0.8 rather than 1 is used because this gives a rather better empirical description of the frequencies in the simple 1D model for short-period superlattices, although this depends on the particular mode (e.g., GaAs or AlAs, LO or TO—see Samson[39]).

It is clear that the measured confined mode frequencies cannot be satisfactorily mapped in this simple way onto the bulk dispersion curves, neither can satisfactory agreement between theory and experiment be obtained without inclusion of the effects of interfacial diffusion. However, it can be seen from Fig. 4 that the inclusion of interfacial broadening $W=1.4$ produces over a wide range of modes and superlattices a very satisfactory agreement between theory and experiment. Particularly significant is the agreement for the shortest period superlattice ($n_1=n_2=2$) measurements, which is distinctly different from both the bulk frequency and the 50% alloy frequency, and the description of the AlAs modes (for which the only mode detectable experimentally is the LO_m mode with index $m=1$). In the latter case, it is apparent that even with this modest degree of interfacial broadening, the local-mode contribution is sufficient to force several of the modes to lie outside the band for [001] LO phonons.

As pointed out in Sec. II A, Raman intensities are less straightforward to model than dielectric strengths, and since we are concentrating in this paper primarily on the mode frequencies, we give only a preliminary assessment of the model's description of Raman intensities. The basic effect of interfacial broadening on the intensities of confined optic modes is to increase the scattering from higher index m modes as W increases. This trend is illustrated in Fig. 5, showing the LO_1 to LO_3-intensity ratio $I_1:I_3$ for a $(GaAs)_7/(AlAs)_7$ superlattice, as obtained from Eq. (22) [with a value of 1.0 for the AlAs (LO_1)- to GaAs (LO_1)-intensity ratio]. The value of the GaAs $I_1:I_3$ ratio is ~ 20 for $W=0$ using the values in Table I, and is very sensitive to the choice of parameters, but becomes much less sensitive when W is of the order of the value found in our samples. For comparison, our measurements (at $W=1.4$) of this ratio give a value of about 3, in tolerable agreement with the model prediction.

It is worth pointing out that the GaAs ratio $I_1:I_3$ at $W=0$ is not equal to the value expected for atomic displacements following a simple sine function. This fact is related to the presence of the Ga-Al interaction ($E_{12}\neq E_{11}\neq E_{22}$) which has an effect on the interface Ga and Al atoms such as to modify their displacements from that of the simple sinelike value. This also explains why the LO and TO intensity ratios are different at $W=0$, since in the TO case $E_{12}\approx E_{11}\approx E_{22}$. Furthermore, as the interface broadening increases the LO mode intensities are more affected than the TO mode intensities (more particularly, I_3 increases). This is largely explained from Fig. 2 where we see that the shift in the LO dispersion curve is far larger than the TO branch for the same change in alloy composition. Hence the confined TO modes are less sensitive (both in frequency and intensity) to the presence of alloy planes at the interface as a result of the broadening.

A more comprehensive set of measurements of the LO_1- to LO_3-intensity ratio has been made by Wicks, Bradshaw, and Radulescu,[6] who examined a series of

$(GaAs)_7/(AlAs)_7$ superlattice samples which had been grown with different growth stops at each heterointerface, thus producing samples which we would characterize with different values of broadening parameter W. Their measurements show clearly the decrease of the ratio as W increases, the general trend of the data being well described by our model.

B. Far-infrared measurements

FIR experiments are capable of directly probing the dielectric susceptibility of a sample, although it is worth emphasizing that it is not straightforward to interpret an infrared reflectivity spectrum without the benefit of modeling the response of the actual sample structure under investigation. Such measurements on some of the samples used for the Raman experiments described above in Sec. III A have already established that the form of Eqs. (25) and (26) is correct.[18,31,32] In particular, oblique incidence reflectivity measurements have shown up dips in the p-polarization spectra at the confined LO frequencies, as measured by Raman scattering, and an increase in the reflectivity at the confined TO frequencies in both polarizations. The overall shape of the resulting spectra have been successfully modeled using a phenomenological form of (25) and (26), with LO_m and TO_1 mode frequencies taken from Raman measurements and first-order oscillator strengths given by the expression

$$S_{s1}^{P}=[(\omega_{s1}^{L})^2-(\omega_{s1}^{T})^2]\beta_s^P \quad (P=\text{L or T}) ,$$

where

$$\beta_s^{L}=\frac{n_s/\epsilon_{\infty,s}}{n_1/\epsilon_{\infty,1}+n_2/\epsilon_{\infty,2}}$$
$$\beta_s^{T}=\frac{n_s\epsilon_{\infty,s}}{n_1\epsilon_{\infty,1}+n_2\epsilon_{\infty,2}} \tag{36}$$

with values $\beta_{GaAs}^{L}=\beta_{AlAs}^{T}=0.438$ and $\beta_{AlAs}^{L}=\beta_{GaAs}^{T}=0.562$ for $n_1=n_2$. Best-fit values were used for higher-order oscillator strengths and confined TO_m frequencies. Attenuated total reflection data have also been fitted using the same parameters. It should be noted that all oscillator strengths quoted in Ref. 18 must be multiplied by β_s^{L} or β_s^{T} to be compatible with the oscillator strengths quoted here.

In our previous publications[18,31,32] we did not attempt to fit FIR data to any microscopic model, although Scamarcio *et al.*[11] have now fitted experimental TO_1 modes to an *ab initio* model. Since all the parameters in (25) and (26) are obtainable from the above model with $Q=0$, we can now make a direct comparison with FIR results. In addition, damping parameters can be calculated according to (30) and trivially introduced into the expressions for ϵ_{xx} and ϵ_{zz} by making the substitution $\omega^2\rightarrow\omega^2+i\omega\Gamma_\mu$ for each mode. In order to obtain ϵ_{xx}^{∞} and ϵ_{zz}^{∞} we resort to a bulk-slab effective-medium type of approach,[33–35] making an appropriate average of the high-frequency dielectric constants ϵ_s^{∞} of the constituent lattices s over the layer concentrations P_{si}:

$$\epsilon_{xx}^{\infty}=\frac{1}{N}\sum_i[P_{1i}\epsilon_1^{\infty}+P_{2i}\epsilon_2^{\infty}] ,$$
$$\frac{1}{\epsilon_{zz}^{\infty}}=\frac{1}{N}\sum_i\frac{1}{[P_{1i}\epsilon_1^{\infty}+P_{2i}\epsilon_2^{\infty}]} . \tag{37}$$

We have used values of 10.9 and 8.5 for ϵ_{GaAs}^{∞} and ϵ_{AlAs}^{∞}, respectively.[20] For damping parameters we have taken Γ_{Ga}, Γ_{Al}, and Γ_{As} all equal to 1 cm^{-1}, and Γ_x^0 equal to 15 cm^{-1} (corresponding to a linewidth in the 50% alloy of ~ 5 cm^{-1}). Figures 6 and 7 show the oblique incidence reflectivity spectra obtained for three superlattices in both s and p polarization, together with theoretical curves obtained using parameters appropriate to superlattices with sharp interfaces and to those with an interfacial broadening of $W=1.4$. It is clear that in the latter case the agreement with experiment is much closer than in the former. It should be noted, however, that part of this apparent improvement when interface broadening is included is because of the significant increase in the calculated damping when alloying occurs. We compare experimental confined TO frequencies with values calculated for $W=1.4$ in Fig. 8, plotted in the same way as the confined LO frequencies shown in Fig. 4. The agreement between theory and experiment is seen to be very close.

Within the GaAs optic region, the spectra are dominated by the response of the substrate, producing the rise in reflectivity around the bulk TO frequency 271 cm^{-1} (preceded by a sharp dip due to interference effects) and the sharp cutoff above the bulk LO frequency 295 cm^{-1}. Most of the remaining prominent features in the reflectivity spectra within both GaAs and AlAs bands occur at either confined TO or confined LO frequencies, corresponding to poles in ϵ_{xx} and zeros in ϵ_{zz}, respectively. However, zeros in ϵ_{xx} and poles in ϵ_{zz}, both of which occur at frequencies that depend on oscillator strengths, do not necessarily produce features in the spectrum.[36] It is therefore not automatically possible to use the frequency of FIR features to measure oscillator strengths, and in order to determine these parameters it is usually necessary to look at the depth of the dips at LO frequencies or the height of the reflectivity increases at TO frequencies. Nevertheless, in the s-polarization measurements, the reflectivity increases around the confined TO frequencies, then drops as $\epsilon_{xx}\rightarrow 0$ at a higher frequency (although the substrate also causes a dip at ~ 270 cm^{-1} within this region for GaAs-like modes); in the case of TO_1, the width of the resulting high-reflectivity region therefore gives an indication of the appropriate oscillator strength. In the GaAs region the frequency at which the TO_1 high-reflectivity region ends is around 280–290 cm^{-1}, and in the AlAs region it is around 380–390 cm^{-1}; the good agreement between theory and experiment at these frequencies suggests that oscillator strengths are being calculated correctly. However, a more precise test of TO_1 oscillator strengths is to use the technique of attenuated total reflection.[37] The results from this technique will be discussed in a separate paper.

The overall damping on each mode can generally be judged from the sharpness of the features around the res-

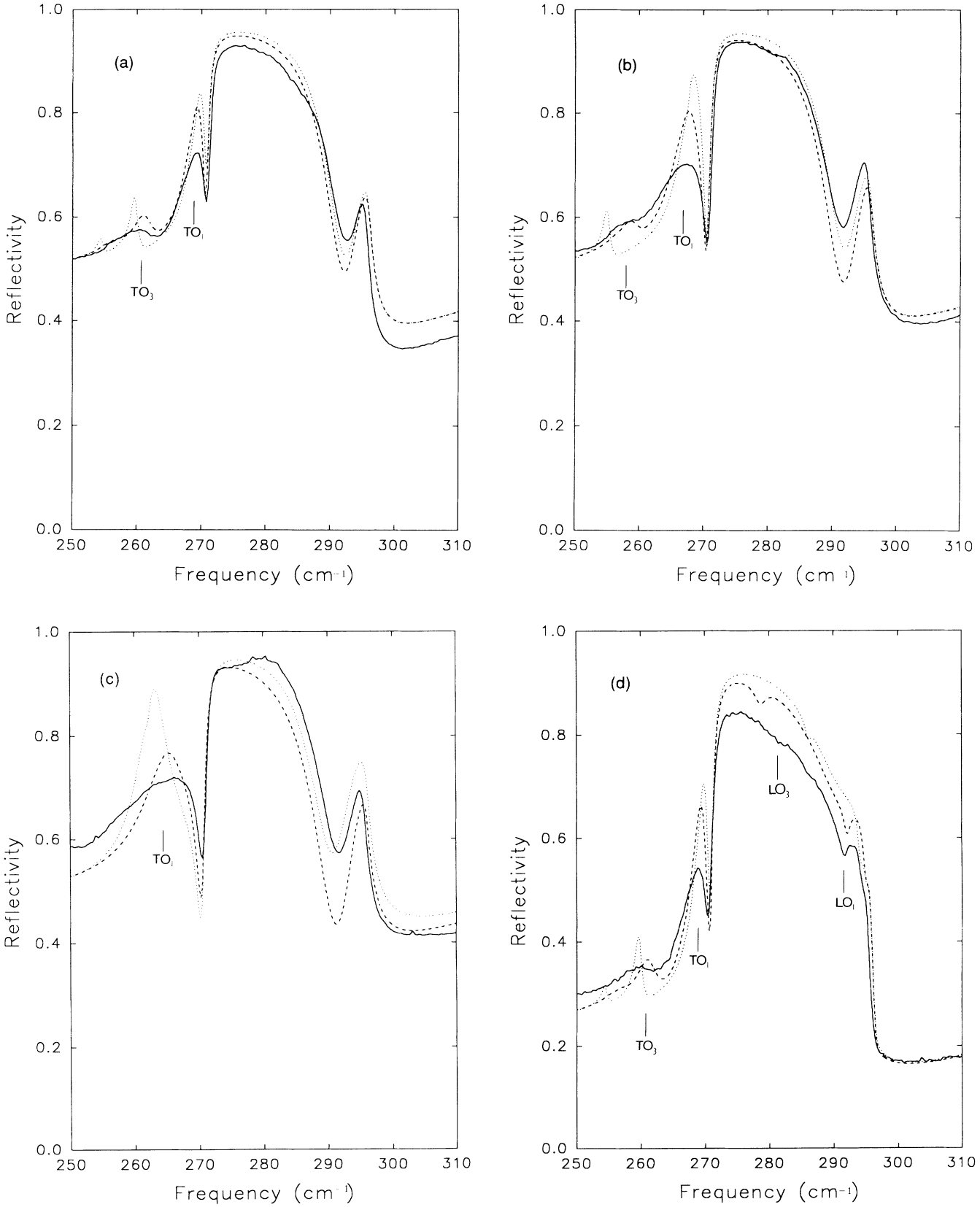

FIG. 6. Comparison of GaAs-like FIR reflectivity spectra with model spectra in $(GaAs)_n/(AlAs)_n$ superlattices. (a) $n=6$, s-polarization; (b) $n=4$, s polarization; (c) $n=2$, s polarization; (d) $n=6$, p polarization (e) $n=4$, p polarization; and (f) $n=2$, p polarization. The curves are experimental (——); theory with $W=1.4$(---); theory with $W=0$(· · · ·). The marked features correspond to experimental confined mode frequencies.

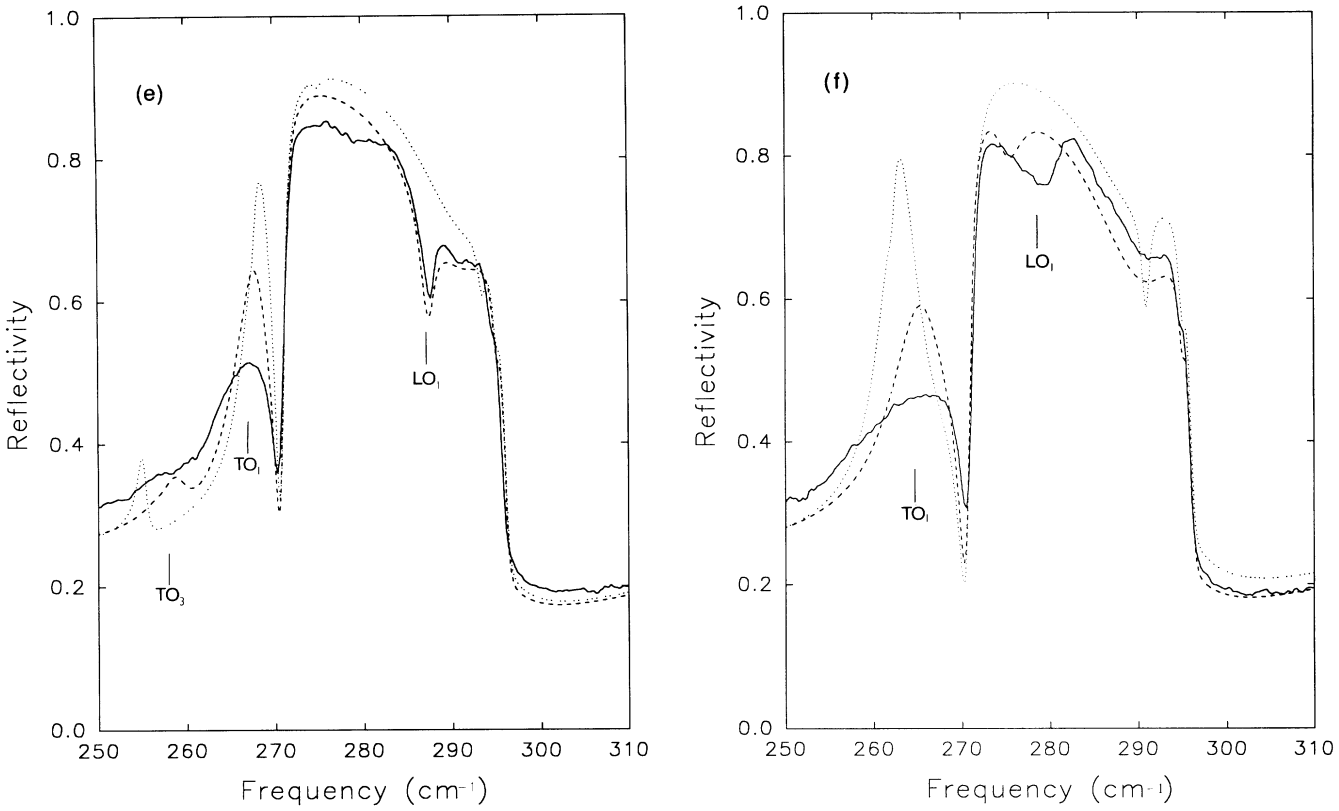

FIG. 6. (*Continued*).

onances. However, in the case of the GaAs TO_1 oscillator the dip at around 290 cm^{-1} in the *s*-polarized spectrum gives additional information.[36] This dip is due to interference between the top and bottom surfaces of the superlattice, and occurs in the region where ϵ_{xx} for the superlattice is positive but ϵ for the GaAs substrate is negative; most of the radiation passing through the superlattice in this frequency region is therefore reflected by the substrate. A dip in the spectrum appears because a portion of the radiation is absorbed by the superlattice, due to TO_1 phonon damping—the greater the damping, therefore, the deeper the dip. It is noticeable that the model appears to underestimate the TO_1 damping when measured according to the sharpness of the features around the TO_1 frequency, but overestimates it when measured according to the depth of the feature at around 290 cm^{-1}. This shows that there is some deviation from the usual form for the damped harmonic oscillator response used in Eqs. (25) and (26), which incorporate single frequency-independent damping parameters Γ_μ for each mode.

An extra point of note in the reflectivity spectrum in the *p*-polarized reflectivity spectrum of the $(GaAs)_4/(AlAs)_4$ sample is the unexpected appearance of a feature at the GaAs-like LO_2 frequency. This may be modeled by assuming a different roughness at the AlAs/GaAs interface from that at the GaAs/AlAs interface,[10] thus causing a lowering of symmetry that allows the even-*m* modes to become infrared active.

IV. CONCLUSIONS

We have introduced a model for phonon modes in GaAs/AlAs superlattices that takes account of interfacial broadening by the use of local-mode coordinates. It is clear that the model can successfully account for discrepancies between measured mode frequencies and calculated frequencies using a model in which imperfect interfaces are assumed, and that the model can be used as a quantitative indicator of the degree of interfacial broadening produced in as-grown semiconductor superlattices. The model can also successfully explain Raman-scattering intensities, infrared dielectric mode strengths, and linewidths. Although the model is applied here to the description of the optic-phonon modes, it can equally well in principle be applied to acoustic modes, where it will give an analysis analogous to that of Jusserand *et al.*[4]

The short-period superlattices, as grown by MBE, give a value $W=1.4$ for the broadening parameter. This value corresponds well with estimates made by x-ray diffraction.[38] Similar x-ray measurements on samples grown under the same conditions as those studied here[39] show that the extent of the interfaces is 3 to 4 monolayers. In the same terms, the value $W=1.4$ from the error function model corresponds to an interface full width of about 3.2 monolayers. This close agreement between two methods of measuring the interface roughness is very reassuring, and also emphasizes the necessity of including

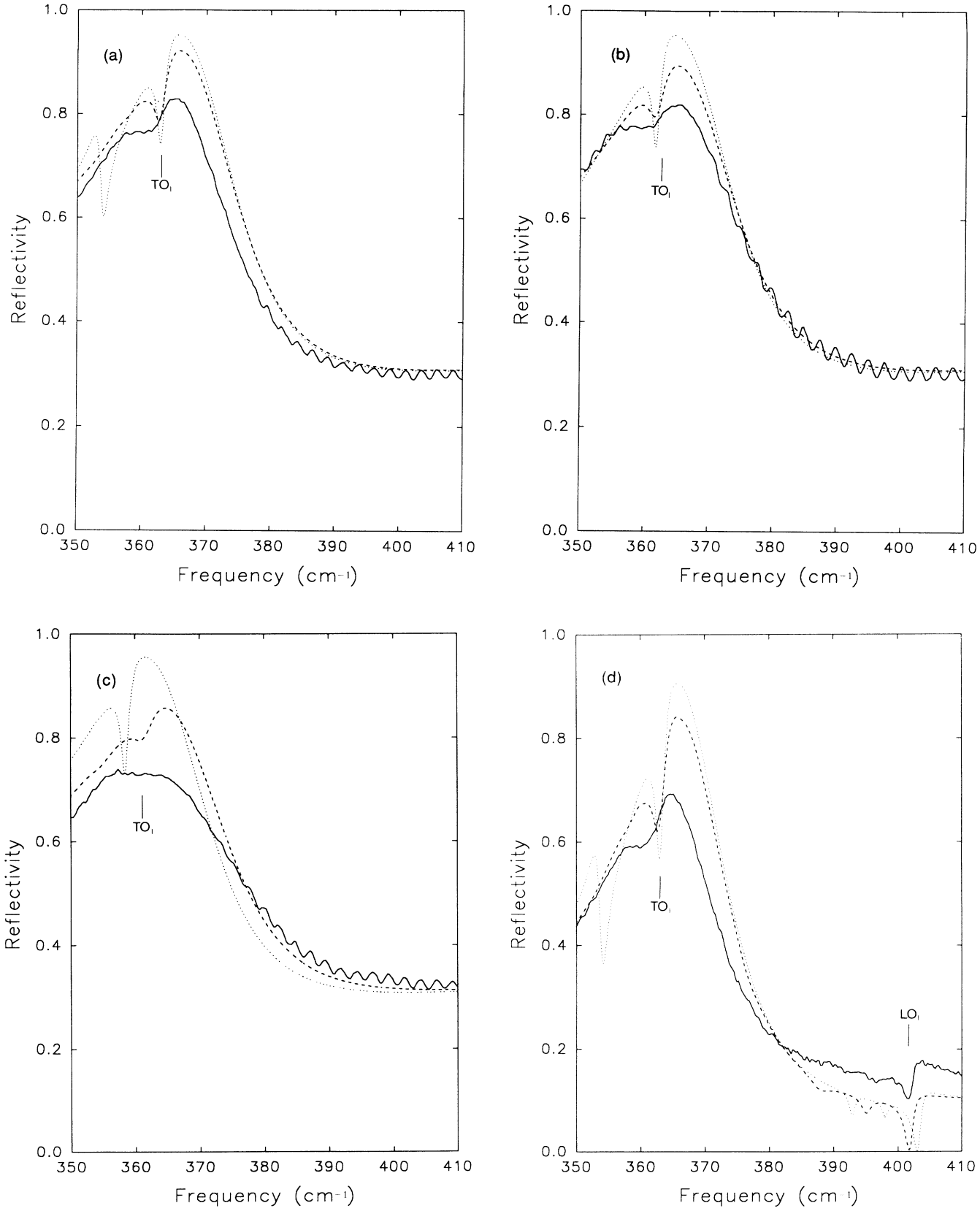

FIG. 7. Comparison of AlAs-like FIR reflectivity spectra with model spectra in $(GaAs)_n/(AlAs)_n$ superlattices. (a) $n=6$, s polarization; (b) $n=4$, s polarization; (c) $n=2$, s polarization; (d) $n=6$, p polarization; (e) $n=4$, p polarization; and (f) $n=2$, p polarization. The curves are experimental (——); theory with $W=1.4$(---); theory with $W=0$ (· · · ·). The marked features correspond to experimental confined mode frequencies.

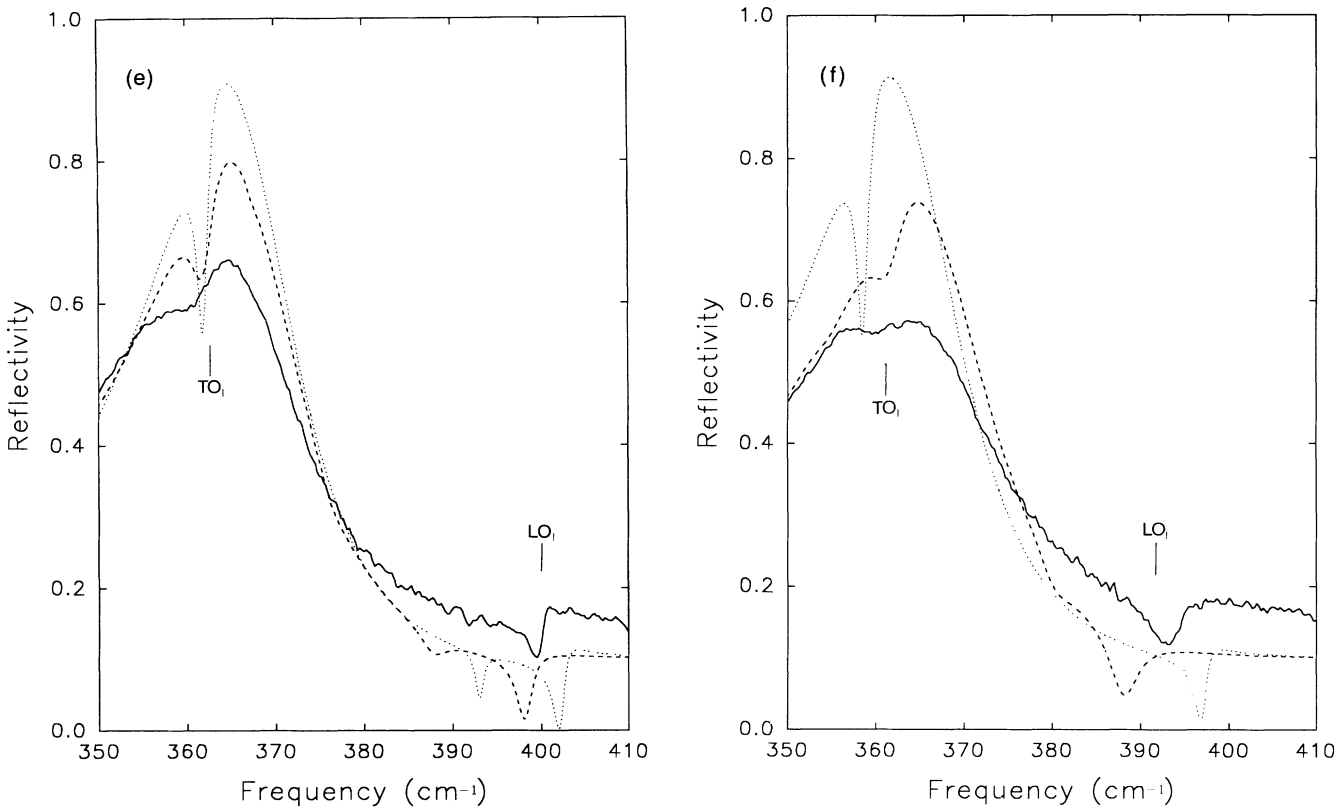

FIG. 7. (*Continued*).

the roughness when attempting to account for the phonon frequencies in short period superlattices. Scanning tunneling microscopy[40] investigations have shown that the apparent interface roughness is caused by terracing in the growth planes; the materials studied here have terraces with lateral dimensions of several monolayers in the growth planes and one monolayer in the growth direction. Our model does not distinguish between the effects of roughness and interatomic diffusion of Ga and Al atoms, but the latter is unlikely to be important in MBE-grown samples using substrate temperatures in the region of those used for our samples (630 °C). A discussion of the effects of atomic-scale surface roughness has recently been given by Jusserand *et al.*;[10] by growing asymmetrically designed samples, these authors have shown that the dominant contribution to surface roughness comes from the "inverse" interface (the growth of a GaAs layer on an AlAs layer). The samples described here are symmetrical in design, in which case the value $W=1.4$ represents a broadening averaged over the two types of interface; for such samples, we have modeled the effects when the broadening is assigned primarily to one interface only (keeping the average W value constant) without seeing any significant shift in mode frequencies.

It is worth reviewing here the principal effects caused by interface broadening, and how they can be given a simple physical interpretation. As far as the frequencies of the modes are concerned, interface broadening has little effect on the folded acoustic phonons simply because there is very little difference between the LA modes of GaAs and AlAs, consequently the primary interest is in the frequency shifts of the confined optic-phonon modes (on the other hand, the *intensities* of the acoustic modes are significantly affected by interface roughness). For the optic modes, there is an increasing degree of admixture of alloylike character into the pure superlattice modes with increasing broadening W. As can be seen from the data in Figs. 4 and 8, the trends are not altogether straightforward: compared to the bulk dispersion curves, the LO modes are shifted downwards in frequency, but the shifts of the TO modes may be either up or down.

The key to the understanding of these differences is the question of whether the effective confinement length l_μ of the phonon mode is increased or decreased by the broadening of the interface—if the former occurs, the confined mode frequencies will increase (longer wavelength implies smaller wave vector and higher frequency), while the opposite is the case if the dimension l_μ of the effective confinement region is reduced. Suppose one approximates the interface region by a layer of width $\sim W$ of the 50% alloy $Al_{0.5}Ga_{0.5}As$. A given confined mode μ will penetrate into the interface region if its frequency ω_μ lies within the band of phonons for the 50% alloy, whereupon the effective confinement length l_μ increases and there is an upward shift to the frequency ω_μ; conversely, if ω_μ lies outside the alloy band, the frequency shift is downwards. The 50% alloy bands are shown in Fig. 2, and it turns out in practice that one can usually use a simpler criterion based only on the appropriate

zone-center frequency ω_a of the 50% alloy, shown in Figs. 4 and 8: if $\omega_\mu < \omega_a$, then ω_μ is increased over the value for the superlattice with sharp interfaces, and if $\omega_\mu > \omega_a$, then ω_μ is decreased. This type of consideration largely explains the behavior of all the modes shown in Figs. 4 and 8, where the agreement between experiment and theory is very satisfactory. Nonetheless, we should recognize that the real situation is more complicated than

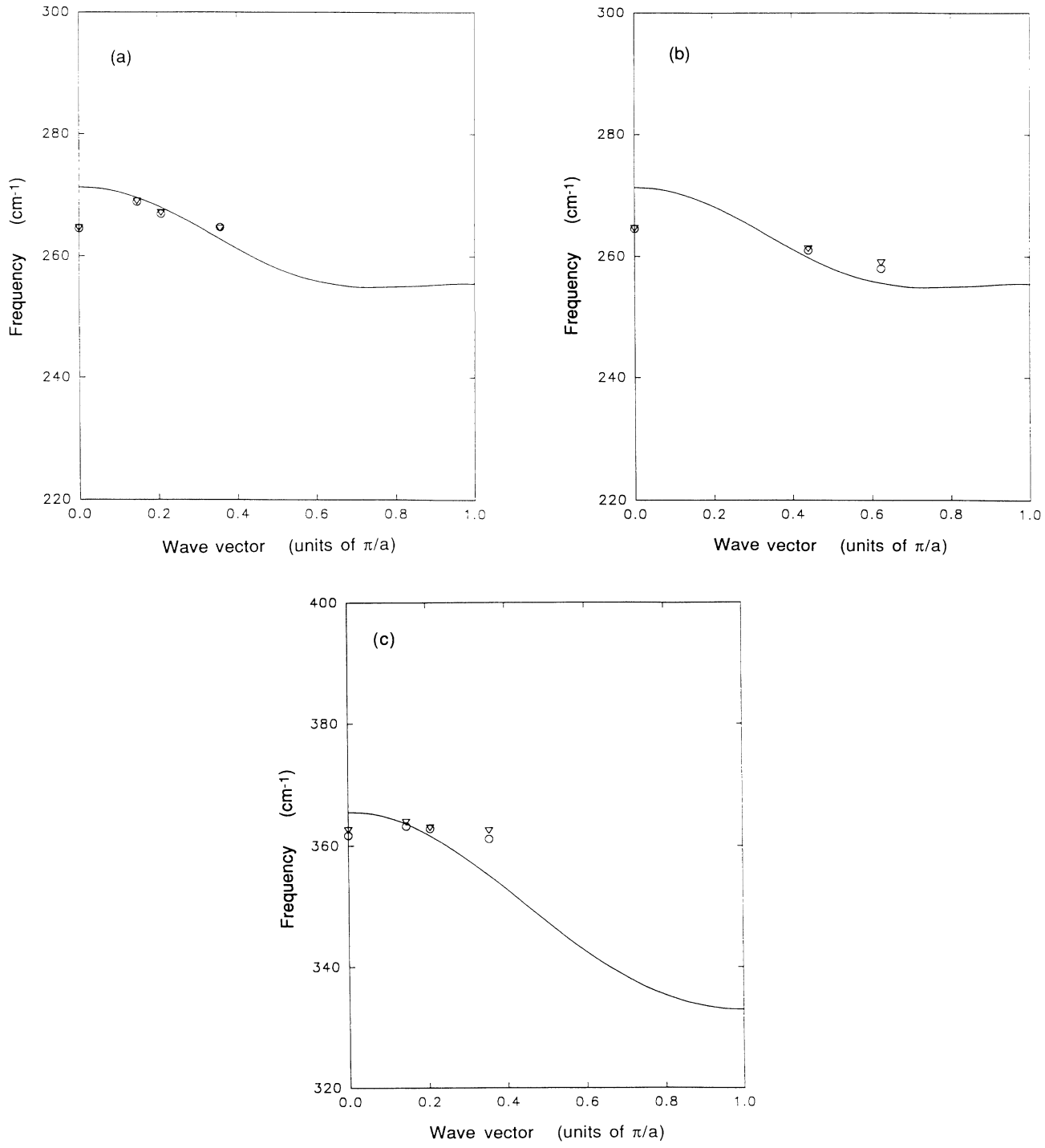

FIG. 8. TO confined mode frequencies in short-period $(GaAs)_n/(AlAs)_n$ superlattices as measured by far infrared reflectivity (○) and as calculated for $W = 1.4$(▽). The data pairs for modes of index m are shown at effective wavevector $q = m/(n + 0.8)$. The solid curves show the bulk dispersion curves for the parameters given in Table I. (a) GaAs-like $m = 1$; (b) GaAs-like $m = 3$; (c) AlAs-like $m = 1$. In each case the alloy $Al_{0.5}Ga_{0.5}As$ is shown for reference at $q = 0$, followed by the superlattice data (from left to right) corresponding to $n = 6$, 4, and 2 (the GaAs-like $m = 3$ mode is not observed for $n = 2$).

this. In particular, when a significant fraction of the confined mode displacement occurs within an alloyed portion of the superlattice (as occurs when the interface roughness is of the order of the layer width) it is no longer sufficient to consider confinement simply on the basis of bulk dispersion curves for the pure materials. This explains why AlAs-like LO's can occur below the edge of the bulk AlAs dispersion curve [see Fig. 4(e)]. In general, such effects are more important for higher index modes.

Molinari *et al.*[12] and Kechrakos, Briddon, and Inkson[15] have made similar comments regarding the difference in behavior of the GaAs and AlAs LO confined modes as a function of increasing interface width. In general, the TO modes are less affected (in frequency, Raman intensity and FIR oscillator strength) by the interface broadening than are the LO modes (Fig. 5), but our modeling shows that the higher-order AlAs TO modes actually increase in frequency as W increases.[41] Unfortunately, although the GaAs-like TO_3 mode is observed, we are not able to resolve the AlAs-like TO_3 mode in any of our FIR data.

In the context of the linewidths of the confined phonon modes, we have compared our predictions with both the Raman and FIR data and find qualitatively good agreement. In general, for a constant W, the linewidth increases as the mode frequency decreases (either as layer thickness decreases or mode index increases). This prediction is in agreement with the ± 1 monolayer model used by Fasol *et al.*,[5] in which the broadening (in longer period superlattices) is assumed to be that caused by an uncertainty of one monolayer in the thickness of the confining layers. However, if one were to compare the linewidths of the GaAs-like LO and TO confined phonons using the ± 1 monolayer model, one would conclude that the latter should have a much smaller linewidth because of the smaller dispersion associated with the TO branch. This conclusion is in disagreement both with the FIR data and with our model, which gives a good account of the data using the same alloy linewidth parameter $\Gamma_x^0 = 15$ cm^{-1} for both the TO and LO data. Nonetheless, we should point out that the actual linewidths of $Al_xGa_{1-x}As$ alloys are considerably more complicated than the semiempirical approach used here (see Jusserand and Sapriel[19]), and require details of the full 3D density of states if modeling is required with any greater degree of realism.

ACKNOWLEDGMENTS

This work has been supported by a Research Grant from the U.K. Science and Engineering Research Council (SERC). One of us (B. S.) acknowledges partial support from SERC.

APPENDIX: COUPLING MATRIX Y

We list here the elements of the coupling matrix **Y** of Eq. (12), using the ten parameters M_1, C_1, E_{11}, D_1, M_2, C_2, E_{22}, D_2, E_{12}, and H introduced in Sec. II (see Table I). A single coordinate vector **e** is used, with $3N$ components (N is the number of layers in the superlattice unit cell), and the correspondence with the individual coordinates e_{Ai}, e_{1i}, and e_{2i} is

$$e_i \equiv e_{Ai}, e_{i+N} \equiv e_{1i}, e_{i+2N} \equiv e_{2i} \quad \text{for } i = 1,2,\ldots,N \ . \tag{A1}$$

The nonzero elements of the coupling matrix **Y** are as follows, where $i = 1,2,\ldots,N$, and $s,s' = 1$ or 2. The notation $[i+1]$ and $[i-1]$ implies that cyclical boundary conditions satisfying Bloch's theorem are to be applied: namely, if the index in brackets [ ] exceeds N, it is to be replaced by 1 and the matrix element multiplied by $e^{2\pi iQ}$ (which is unity for zone-center modes), with a similar replacement of $[i-1]$ by N when $i = 1$ and multiplication by $e^{-2\pi iQ}$.

$$\begin{aligned}
Y_{i,i} &= (P_{1,i} + P_{1,[i+1]})(C_1 + D_1) \\
&\quad + (P_{2,i} + P_{2,[i+1]})(C_2 + D_2) \ , \\
Y_{i,[i-1]} &= -(P_{1,i} D_1 + P_{2,i} D_2) \ , \\
Y_{i,[i+1]} &= -(P_{1,[i+1]} D_1 + P_{2,[i+1]} D_2) \ , \\
Y_{i,i+Ns} &= -C_s \sqrt{P_{s,i}/M_s} \ , \\
Y_{i,[i+1]+Ns} &= -C_s \sqrt{P_{s,[i+1]}/M_s} \ , \\
Y_{i+Ns,i+Ns} &= M_s^{-1}[2C_s + E_{s1}(P_{1,[i-1]} + P_{1,[i+1]}) \\
&\quad + E_{s2}(P_{2,[i-1]} + P_{2,[i+1]}) + HP_{\bar{s}i}] \ , \\
Y_{i+Ns,i+N\bar{s}} &= -H\sqrt{P_{s,i}P_{\bar{s},i}/M_s M_{\bar{s}}} \ , \\
Y_{i+Ns,[i\pm1]+Ns'} &= -E_{ss'}\sqrt{P_{s,i}P_{s',[i\pm1]}/M_s M_{s'}} \ , \\
Y_{i+Ns,i} &= Y_{i,i+Ns} \ , \\
Y_{i+Ns,[i-1]} &= Y_{[i-1],i+N} \ .
\end{aligned} \tag{A2}$$

*Present address: Optoelectronics Research Centre, University of Southampton, SO9 5NH United Kingdom.
†Present address: Department of Physics, University of Nottingham, Nottingham, NG7 2RD United Kingdom.
‡Present address: Department of Physics, Manchester Polytechnic, Manchester, M1 5GD United Kingdom.

[1] B. Jusserand and M. Cardona, in *Light Scattering in Solids, V*, edited by M. Cardona and G. Güntherodt (Springer, Berlin, 1989), p. 49.
[2] J. Menendez, J. Lumin. **44**, 285 (1989).
[3] A. Fasolino, E. Molinari, and K. Kunc, Phys. Rev. B **41**, 8302 (1990).
[4] B. Jusserand, F. Alexandre, D. Pacquet, and G. LeRoux, Appl. Phys. Lett. **47**, 301 (1985).
[5] G. Fasol, M. Tanaka, H. Sakaki, and Y. Horikoshi, Phys. Rev. B **38**, 6065 (1988).
[6] G. W. Wicks, J. T. Bradshaw, and D. C. Radulescu, Appl. Phys. Lett. **52**, 570 (1988).
[7] S. Baroni, P. Giannozzi, and E. Molinari, Phys. Rev. B **41**, 3870 (1990).

[8]C. A. Warwick, W. Y. Jan, A. Ourmazd, and T. D. Harris, Appl. Phys. Lett. **56**, 2666 (1990).
[9]D. Gammon, B. V. Shaabrook, and D. S. Katzer, Appl. Phys. Lett. **56**, 2710 (1990).
[10]B. Jusserand, F. Mollot, J.-M. Moison, and G. LeRoux, Appl. Phys. Lett. **57**, 560 (1990); J. M. Moison, C. Guille, F. Houzay, F. Barthe, and M. Van Rompay, Phys. Rev. B **40**, 6149 (1989).
[11]G. Scamarcio, L. Tapfer, W. Konig, A. Fischer, K. Ploog, E. Molinari, S. Baroni, P. Giannozzi, and S. de Gironcoli, Phys. Rev. B **43**, 14 754 (1991).
[12]E. Molinari, S. Baroni, P. Giannozzi, and S. de Gironcoli, *Proceedings of the 20th International Conference on the Physics of Semiconductors,* edited by E. M. Anastassakis and J. D. Joannopoulos (World Scientific, Singapore, 1990), p. 1429; Phys. Rev. B **45**, 4280 (1992).
[13]S. Baroni, S. de Gironcoli, and P. Giannozzi, Phys. Rev. Lett. **65**, 84 (1990).
[14]B. Jusserand, D. Pacquet, and F. Mollot, Phys. Rev. Lett. **63**, 2397 (1989).
[15]D. Kechrakos, P. R. Briddon, and J. C. Inkson, Phys. Rev. B **44**, 9114 (1991).
[16]I. F. Chang and S. S. Mitra, Phys. Rev. B **2**, 1215 (1970); I. F. Chang and S. S. Mitra, Adv. Phys. **20**, 359 (1971).
[17]B. Samson, S. R. P. Smith, C. T. Foxon, D. Hilton, and K. J. Moore, Solid State Commun. **78**, 325 (1991).
[18]T. Dumelow, A. A. Hamilton, K. A. Maslin, T. J. Parker, B. Samson, S. R. P. Smith, D. R. Tilley, R. B. Beall, C. T. B. Foxon, J. J. Harris, D. Hilton, and K. J. Moore, in *Light Scattering in Solids,* edited by D. J. Lockwood and J. Young (Plenum, New York, 1991), p. 461.
[19]B. Jusserand and J. Sapriel, Phys. Rev. B **24**, 7194 (1981).
[20]O. K. Kim and W. G. Spitzer, J. Appl. Phys. **50**, 4362 (1979).
[21]D. Strauch and B. Dorner, J. Phys. Condens. Matter **2**, 1457 (1990).
[22]A. Onton and R. J. Chicotka, Phys. Rev. B **10**, 591 (1974).
[23]B. Monemar, Phys. Rev. B **8**, 5711 (1973).
[24]H. Chu, S.-F. Ren, and Y.-C. Chang, Phys. Rev. B **37**, 10 746 (1988).
[25]D. Levi, Shu-Lin Zhang, M. V. Klein, J. Klem, and H. Morkoc, Phys. Rev. B **36**, 8032 (1987).
[26]R. M. Fleming, D. B. McWhan, A. C. Gossard, W. Wigmann, and R. A. Logan, J. Appl. Phys. **51**, 357 (1980).
[27]K. J. Moore, G. Duggan, P. Dawson, and C. T. Foxon, Phys. Rev. B **38**, 5535 (1988).
[28]G. W. Chantry, H. M. Evans, J. Chamberlain, and H. A. Gebbie, Infrared Phys. **9**, 85 (1969).
[29]T. Dumelow, A. A. Hamilton, K. A. Maslin, T. J. Parker, D. R. Tilley, R. B. Beall, C. T. B. Foxon, J. J. Harris, D. Hilton, and K. J. Moore, in *Proceedings of International Workship on Fourier Transform Infrared Spectroscopy, Antwerp, 1990,* edited by E. F. Vansant (University of Antwerp, Belgium 1990), p. 141.
[30]B. Jusserand and D. Pacquet, Phys. Rev. Lett. **56**, 1752 (1986).
[31]T. Dumelow, A. R. El Gohary, A. A. Hamilton, K. A. Maslin, T. J. Parker, N. Raj, B. Samson, S. R. P. Smith, D. R. Tilley, P. J. Dobson, C. T. B. Foxon, D. Hilton, and K. J. Moore, Mater. Sci. Eng. B **5**, 205 (1990).
[32]T. Dumelow, A. A. Hamilton, T. J. Parker, D. R. Tilley, C. T. B. Foxon, D. Hilton, and K. J. Moore, Int. J. Infrared Millimeter Waves **11**, 901 (1990).
[33]S. M. Rytov, Zh. Eksp. Teor. Fiz. **29**, 605 (1955) [Sov. Phys. JETP **2**, 466 (1956)].
[34]V. M. Agranovich and V. E. Kravtsov, Solid State Commun. **55**, 85 (1985).
[35]N. Raj and D. R. Tilley, Solid State Commun. **55**, 373 (1985).
[36]T. Dumelow and D. R. Tilley (unpublished).
[37]T. Dumelow, A. A. Hamilton, T. J. Parker, D. R. Tilley, R. B. Beall, J. J. Harris, D. Hilton, K. J. Moore, and C. T. B. Foxon, *Proceedings of the International Conference on Optical Characterisation of Semiconductors, Sofia, 1990,* edited by D. B. Kilshev (Trans Tech, Zürich, Switzerland, 1992), p. 191.
[38]P. F. Fewster, J. Appl. Cryst. **21**, 524 (1988); P. F. Fewster, N. L. Andrew, and C. J. Curling (unpublished).
[39]P. F. Fewster (private communication).
[40]M. D. Pashley, K. W. Haberern, W. Friday, J. M. Woodall, and P. W. Kirchner, Phys. Rev. Lett. **60**, 2176 (1988).
[41]B. Samson, Ph.D. thesis, University of Essex, 1991.